

# Little Earth Experiment: an instrument to model planetary cores

Kélig Aujogue<sup>1,\*</sup>, Alban Pothérat<sup>1</sup>, Ian Bates<sup>1</sup>, François Debray<sup>2</sup>, and Binod Sreenivasan<sup>3</sup>

<sup>1</sup> *Applied Mathematics Research Centre, Coventry University, priory street CV1 5FB, UK*

<sup>2</sup> *Laboratoire National des Champs Magnétiques Intenses-Grenoble, CNRS/UJF and*

<sup>3</sup> *Centre for Earth Sciences, Indian Institute of Science, Bangalore 560 012, India.*

(Dated: June 7, 2016)

In this paper, we present a new experimental facility, Little Earth Experiment, designed to study the hydrodynamics of liquid planetary cores. The main novelty of this apparatus is that a transparent electrically conducting electrolyte is subject to extremely high magnetic fields (up to 10T) to produce electromagnetic effects comparable to those produced by moderate magnetic fields in planetary cores. This technique makes it possible to visualise for the first time the coupling between the principal forces in a convection-driven dynamo by means of Particle Image Velocimetry (PIV) in a geometry relevant to planets. We first present the technology that enables us to generate these forces and implement PIV in a high magnetic field environment. We then show that the magnetic field drastically changes the structure of convective plumes in a configuration relevant to the tangent cylinder region of the Earth's core.

PACS numbers: Valid PACS appear here

## I. INTRODUCTION

The magnetic field of planets such as Earth is thought to be generated by dynamo action in their cores. Fluid motion in the Earth's core takes place by a combination of chemical and thermal convection. While chemical convection originates from the release of light elements from the boundary of the inner core, thermal convection originates from secular cooling due to heat loss through the core-mantle boundary, and partly from latent heat release from the inner core boundary. The rotation of the Earth naturally divides convection into two regions, outside and inside the tangent cylinder. The tangent cylinder is an imaginary cylinder aligned with the Earth's rotation axis and touching the solid iron inner core of size 1220 km. The dynamics within the tangent cylinder is of significant interest in geophysics because of observations of the secular variation of the Earth's magnetic field that point to the possible existence of anticyclonic polar vortices in the Earth's core [1, 2]. The origin of these vortices has been investigated by non-magnetic experiments [3] and by a combination of dynamo simulations and the theory of rotating magnetoconvection [4, 5]. Magnetoconvection in a rotating plane layer takes the form of thin viscous columns or large-scale structures [6]. Non-magnetic experiments [3] suggest that thin viscous plumes give rise to a polar vortex via a thermal wind [7]. Nonlinear dynamo simulations, on the other hand, show that magnetic convection within the tangent cylinder is dominated by one or more off-axis plumes that extend from the inner core boundary to the polar region [8]. Such a form of convection produces a strong, but non-axisymmetric polar vortex. It is therefore clear from simulations that the self-generated magnetic field in the

Earth's core has an important role in determining the structure of polar convection.

The effect of a magnetic field alone on convection in an electrically conducting fluid is known to be stabilising from Chandrasekhar's [6] early theory for the infinite plane layer, from experiments in liquid metals [9, 10], and more recently, experiments in electrolytes [11]. The combined effect of the magnetic field and rotation, by contrast, is less straightforward and has received much less attention from experimentalists until now. The main experimental results were obtained in opaque liquid metals, in a plane configuration: [12 and 10] both highlight the change in the size of convective structures due to the magnetic field and show how heat transfer above onset depends on the magnetic field intensity and the rotation rate. Nevertheless, the geometry used in these experiments is not relevant to the Earth's tangent cylinder and liquid metals do not allow extensive flow mapping.

The principal force balance in the Earth's core is between the buoyancy (Archimedean) force that drives fluid motion, the Coriolis force that arises from background rotation and the Magnetic (Lorentz) force that arises from the interaction between the induced electric currents and magnetic fields. Nonlinear inertial and viscous forces are not thought to be important in the rapidly rotating regime of the core. Rotating dynamo models [13–15] are currently our only source of information about the distribution of the so-called MAC forces in the core. Because of the computational effort involved in solving the dynamo equations, rapidly rotating regimes of low Ekman number (ratio of viscous to Coriolis forces,  $\sim 10^{-15}$  for the Earth's core) cannot be reached. As Ekman numbers less than  $\sim 10^{-5}$  have not been systematically explored by simulations, it is not clear that an asymptotic regime independent of the diffusivities will ever be reached. Moreover, simulations suggest that the field distribution in the tangent cylinder is far from uniform, the effect of which is not easy to understand from nonlinear dynamo

---

\* aujoguek@uni.coventry.ac.uk

models. Although the dimensionless field strength in the core (measured by the Elsasser number  $\Lambda$ , the ratio of Lorentz to Coriolis forces) is likely to be of  $\sim 1$  from a global magnetostrophic balance [16, 17], field inhomogeneities could alter the dynamics locally, an effect not obviously understood from dynamo models at moderate to high Ekman number. Laboratory experiments with externally imposed magnetic fields offer a way out of these difficulties by allowing a systematic exploration of low Ekman numbers with uniform as well as non-uniform magnetic fields. The use of a transparent electrolyte as the working fluid offers the additional advantage of visualizing the magnetohydrodynamic (MHD) flows under rotation, which is rendered practically impossible by the opacity of liquid metals.

To elucidate the structure of rotating magneto-convective vortices in the tangent cylinder, a sufficiently flexible apparatus is needed that satisfies the antagonistic design constraints imposed by magnetic fields and rotation, and at the same time, provides a detailed quantitative mapping of the velocity and temperature fields in an Earth-like geometry. The purpose of the present paper is precisely to present such a set-up and to show that it is able to capture some of the basic physical features of the flow in the tangent cylinder. Our apparatus uses a transparent electrolyte with the highest possible electric conductivity in order to reproduce the MHD regime in the core at sufficiently low Ekman number, whilst still being able to visualise the flow with a laser-based technique such as PIV. Since even the best electrolytes are typically a factor  $\sim 10^4$  less conducting than liquid metals, this can only be achieved with magnetic fields typically  $\sim 10^2$  times stronger than those in previous liquid metal experiments. For this reason, the apparatus is operated at the Grenoble High Magnetic Field Laboratory, currently the only facility in the world to offer axial magnetic fields of the order of 10 T in a bore large enough to accommodate our apparatus. Our experiment involves rotating a large mechanical device in a very high magnetic field. The challenge in designing the set-up lies in simultaneously catering for the following:

1. High magnetic field: This requires that all moving parts, including heating elements, must be non-metallic to avoid induced currents and a potentially large braking torque.
2. Rotation: Transmitting torque inside a magnetic field and exchanging data and fluid between the stationary frame and rotating cell is challenging.
3. Sulphuric acid (electrolyte) at high concentration: Most materials have to be chemically resistant and safety procedures add constraints to the design.

The paper is organised in 4 main sections. Section II introduces the general layout of the experiment and the key design elements generating the buoyancy, Coriolis and Lorentz forces. The instrumentation and measurement

techniques implemented are detailed in section III, while section IV presents some typical features of convection in the tangent cylinder which the set-up has been able to reveal. Section V summarizes our findings and gives the scope for future work.

## II. APPARATUS DESIGN

### A. General layout of the experiment

At the heart of the apparatus is the main vessel made of a hemispherical glass dome filled with sulphuric acid ( $H_2SO_4$  of 30% mass concentration), heated at its centre by a cylindrical heating element, cooled on the outside and spun inside a high magnetic field. These functionalities are achieved and monitored thanks to three subsystems: the magnet, the driving system, and the main vessel with its data acquisition system. The key principle of the design is the modularity. The apparatus is designed to the study of the liquid core of the Earth and other planets in the widest possible parameter regimes.

The shape of the vessel and the heating element can potentially be modified to model planets other than the Earth without going through any re-design of the rest of the apparatus. Figure 1 gives a schematic of the apparatus with all subsystems. The driving system is made of a DC motor (DOGA Model 111 E 22) with a belt and pulley arrangement. The main vessel comprises a 300mm diameter PVC turntable bounded by a cylindrical outer shell and supporting a 4mm thick glass dome. The dome has an inner diameter of 276mm and is filled with sulphuric acid. At the centre of the dome, a cylindrical heating element is used to generate convection. The data acquisition system includes a thermocouple data logger, a charge coupled device (CCD) camera (Point Grey Flea 3), a wirelessly triggered laser and a mobile workstation (laptop) rotating with the set-up used to record data from the camera and control the laser. This equipment allows both temperature and PIV measurements. The whole system is approximately 5 m in height. We shall now describe how the apparatus is designed to generate the principal body forces within the constraints laid out in Section I.

### B. Generating the Coriolis force

The Coriolis force is produced by spinning the experimental set-up. The rotation is produced by a DC motor placed at the bottom of the set-up, close to the axis of the solenoidal magnet in order to minimise its exposure to stray field. Figure 1 gives a schematic of the driving module, highlighting the main mechanical components. Motion is transmitted from the DC motor to the main vessel via a belt and a shaft connected to a shaft drive. The shaft drive connects to the main vessel module and

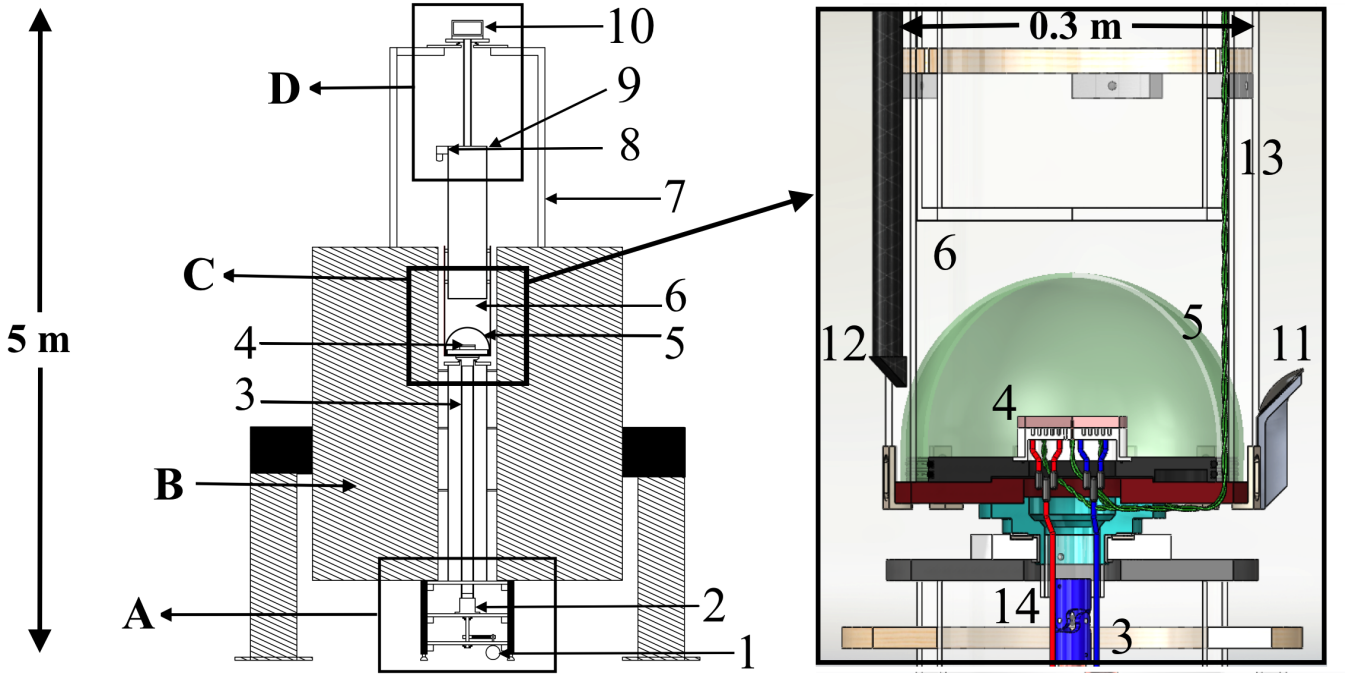


FIG. 1: Left panel: Schematic of the complete system inside a 10 T, 376mm bore Magnet (scale: 1:50). Right panel: Detailed drawing of the main vessel. A. Driving module B. 10T magnet C. Main Vessel D. Measurement system 1. Motor 2. Rotary Union 3. Torque tube 4. Liquid Heater 5. Dome 6. Cooling Water 7. Supporting structure 8. PIV Camera 9. Optical speed sensor 10. Wirelessly controlled mobile workstation recording data in the rotating frame 11. Mirror 12. Laser diode 13. K-type thermocouples connected under and in the ceramic plate 14. Pipe carrying ethylene glycol.

only transmits torque to it. The weight of the main vessel is separately supported by a bearing attached to a fixed horizontal plate resting on the chassis of the driving module via an external tube (figure 1). This design offers a simple and efficient damping system, eliminating the transmission of vibrations from the motor to the main vessel. The same principle is applied to support and rotate the acquisition system located outside the magnet, above the main vessel. The angular velocity of the main vessel  $\Omega$  is set by controlling the voltage applied to the DC motor. The built-in 1 : 2.5 gearbox provides a close-to-linear relation between the output of the regulated DC power supply and the angular velocity of the rotating part of the apparatus. Velocity variations are measured in a range between 2% at high speeds ( $> 1$  revolutions per second) and 6% at lower speeds ( $< 0.5$  revolutions per second). The angular velocity is continuously monitored with the built-in optical system, made of a 72-teeth wheel placed just above the turntable and an optical detector fitted to the magnet bore (see electrical sketch in figure 2).

With the belt/pulley combination, an angular velocity of 2 revolutions per second is reached.

### C. Generating the Buoyancy Force: the rotating heater

The buoyancy force results from an imposed temperature difference between the outside surface of the glass dome and the heating element located at the bottom centre of the fluid volume (Figure 1). As the experiment is rotating inside a magnetic field, it is necessary to build a non-magnetic rotating heating system, as currents circulating in a high magnetic field can cause a mechanical overload of the drive system. For this reason, the heating element is designed as a heat exchanger fed by a heating fluid. The fluid is electrically heated outside the field region in the static frame and pumped to the rotating frame through a rotary union which is built with electrically insulating rotating elements. The heat is released to the working fluid through the heating element.

Figure 3 describes the different elements of the corresponding heating circuit, both static (circulating pump, electric heater, and header tank to pressurise the hydraulic circuit) and rotating (rotary union and heating element). A peristaltic pump (WMC pump UIM243L02BT) guarantees a constant flow rate of heating fluid through the circuit (100 ml/min). We choose ethylene glycol as the heating fluid because of its high heat capacity ( $c_p = 149.5 \text{ J mol}^{-1} \text{ K}^{-1}$ ) and reasonably low viscosity ( $\nu = 1.4 \times 10^{-6} \text{ m}^2 \text{ s}^{-1}$ ).

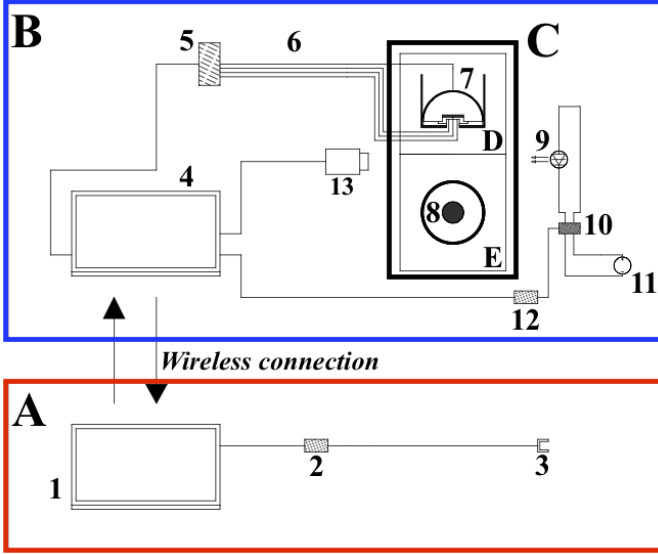


FIG. 2: Schematic of the electrical circuit. A. Static frame (red) B. Rotating frame (blue) C. Main vessel D. Vertical plane E. Horizontal Plane 1. Fixed workstation, 4. Mobile workstation 2. Arduino Uno, 3. Optical speed sensor 5. Data logger 6. Four K-type thermocouples, 7. Glass dome, 8. Liquid heater 9. Laser diode 10. Current controller 11. Battery 12. Arduino Leonardo 13. Camera.

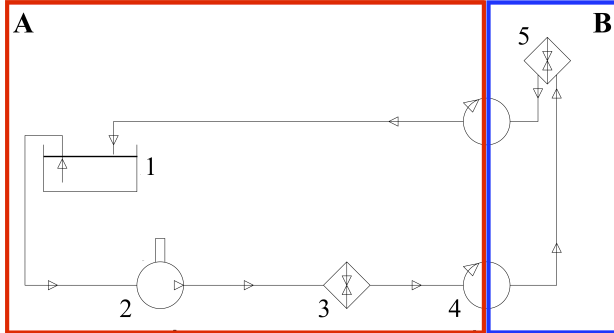


FIG. 3: Schematic of the heating system showing the path of the heating fluid. A. Static frame B. Rotating frame 1. Header tank 2. Pump 3. Electric heater 4. Rotary union and 5. Liquid heater

A purpose-built rotary union connects the static and the rotating frames with a static aluminum housing and a rotating polyvinylidene fluoride (PVDF) shaft. Design of the heating element is technically challenging as it needs to be electrically insulating, resist prolonged exposure to acid and have high thermal conductivity. In view of these opposing constraints, it is designed in two parts: a PVDF base (figure 4) and a high thermal conductivity ceramic lid (made of SHAPAL®, of thermal conductivity  $k_S = 92 \text{ W m}^{-1} \text{ K}^{-1}$ )

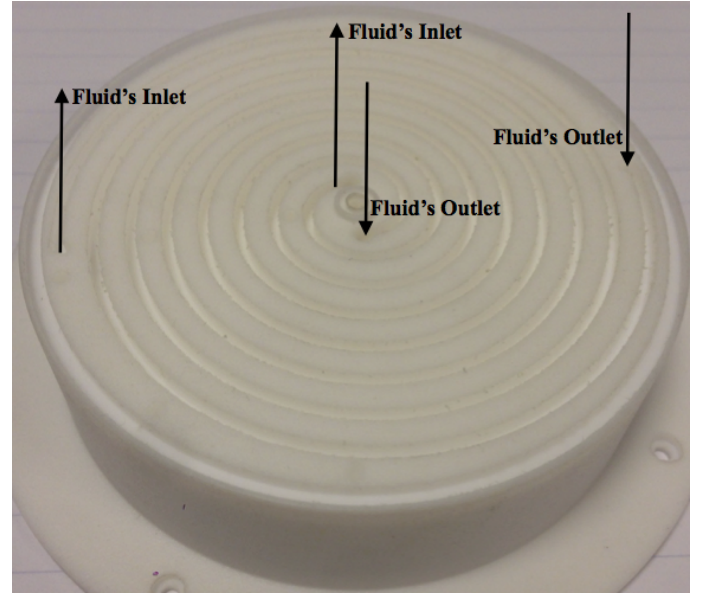


FIG. 4: PVDF base of the liquid operated heater showing the double spiral circulating the heating fluid (ethylene glycol) below the ceramic element (not shown)

Figure 4 shows the base of the PVDF part, where ethylene glycol circulates inside two spiral ducts. The fluid follows two interwoven spirals in opposite directions (inside-out and outside-in), to minimise the inhomogeneity of the temperature. Above this part, the ceramic lid provides a homogeneous temperature boundary in contact with the sulphuric acid. The lid is a circular plate of diameter 0.098 m, reproducing the radius ratio  $\eta$  of the spherical shell core of the Earth ( $\eta_{\text{earth}} = 0.35$  and  $\eta_{\text{exp}} = 0.355$ ). The Biot number  $Bi$  (which measures the ratio of the thermal resistance of the plate to the liquid above it) provides us with an indication of the relative temperature non-uniformity at the upper lid surface (Ozisik [18]; Aurnou & Olson [12]). For a 10mm thick ceramic plate,

$$Bi = \frac{L_{\text{ceramic}}/k_S}{L_{\text{H}_2\text{SO}_4}/k_{\text{H}_2\text{SO}_4}} = \frac{0.01/92}{0.138/0.5} = 3.94 \times 10^{-4}. \quad (1)$$

The boundary between the ceramic and the fluid can therefore be considered isothermal. In addition, numerical simulation of the heat distribution through the ceramic element yields a relative non-uniformity of  $\pm 0.1\%$  at the interface between the fluid and heater, consistent with the prediction from 1.

The outside temperature of the dome is kept constant by placing a sufficiently large volume of water above it. The inhomogeneity in temperature at the dome surface is measured using thermocouples placed on the surface and found to lie in the range  $1^\circ \text{C}$  for an imposed temperature difference between the top of the ceramic and the top of the dome of  $15^\circ \text{C}$ . Within the region of the tangent cylinder, the inhomogeneity drops to  $0.05^\circ \text{C}$ .

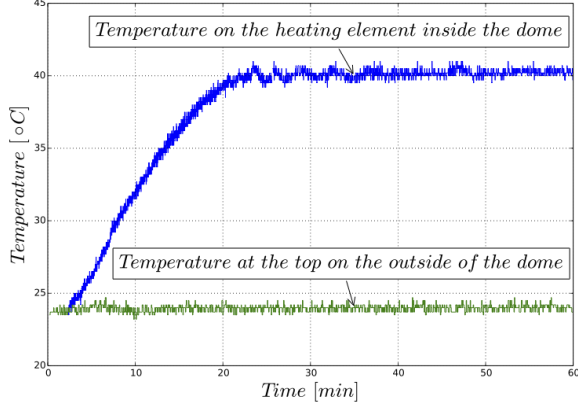


FIG. 5: Evolution of temperature at the top of the dome and the heated ceramic element at the centre of the dome. The imposed temperature difference is 15 °C.

During operation, the temperature at the surface of the heating element is monitored by a thermocouple embedded in the element placed 1 mm below the surface. The temperature at the surface of the dome is not directly measured so that the top view is not obstructed. Instead, the temperature is measured inside the cooling tank above the dome. Figure 5 shows an example of the evolution of the temperature at the heater and the temperature measured at the dome surface. The system has a large thermal inertia and reaches thermal equilibrium after approximately half an hour. After this initial transient, the fluctuations of the temperature difference  $\Delta T$  between heating element and outside cylinder remain of the order of  $\pm 0.1$  K and cannot be correlated to fluctuations in the velocity field. It is therefore not necessary to actively regulate the system after thermal equilibrium is reached.

#### D. Generating the magnetic Lorentz force

The Lorentz force is produced by the interaction between a strong magnetic field and the electric current induced by the convective motion of the fluid. To generate the magnetic field, we use two different magnets: a superconducting magnet and a resistive magnet. The superconducting magnet has a bore of 0.460 m and is 1.2m high. It can be operated at field strengths of 0–4 T. The resistive magnet has a bore of 0.376m and can be operated at 0–10 T.

The key to generating the strongest Lorentz force is the choice of a transparent, Newtonian fluid with the highest possible electrical conductivity and the lowest possible kinematic viscosity, so that the effects of rotation and magnetic field are maximised. We choose sulphuric acid as in [11, 19], as it has a maximum conductivity of  $\sigma = 0.8$  Sm for a mass concentration of 30% at 26.7 °C, with the same transparency as water (see Figure 6 and [20]).

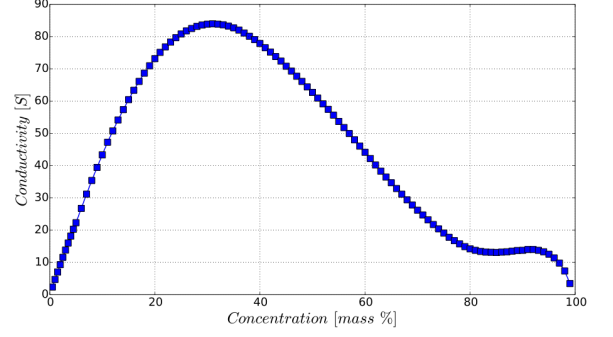


FIG. 6: Variation of the electrical conductivity  $\sigma$  of sulphuric acid with mass concentration at 27.6° C, from Darling [20].

The conductivity of electrolytes varies non-monotonically with their concentration and often exhibits a maximum resulting from the best compromise between a good density of free charge and sufficient ion mobility. Among electrolytes, sulphuric acid presents the highest peak in conductivity. Furthermore, it is relatively safe to handle, compared to other acidic solutions of comparable conductivity. The penalty is a higher viscosity than water ( $\nu_{\text{H}_2\text{SO}_4} = 2.04 \times 10^{-6} \text{ m}^2 \text{ s}^{-1}$ ), which we shall have to compensate by rotating the apparatus at a higher angular velocity, to allow comparisons with non-magnetic experiments where the apparatus is operated with water.

#### E. Physical range of parameters

The range of operation of the apparatus (and its relevance to geophysical problems) is gauged by the realizable values of the five dimensionless parameters that control the MHD regime in rotating planetary cores – Ekman number (E), Rayleigh number ( $Ra$ ), Elsasser number ( $\Lambda$ ), Prandtl number ( $Pr$ ) and magnetic Prandtl number ( $Pm$ ), defined as follows:

$$E = \frac{\nu}{\Omega d^2}, Ra = \frac{g \alpha \Delta T d^3}{\nu \kappa}, \Lambda = \frac{B^2}{\Omega \rho \mu_0 \eta}, Pr = \frac{\nu}{\kappa}, Pm = \frac{\nu}{\eta}, \quad (2)$$

where  $d$  is the characteristic lengthscale,  $\nu$  is the kinematic viscosity,  $\rho$  is the density,  $\kappa$  is the thermal diffusivity,  $\eta = (\mu_0 \sigma)^{-1}$  is the magnetic diffusivity,  $\alpha$  is the coefficient of thermal expansion,  $g$  is the gravitational acceleration,  $\Omega$  is the angular velocity of background rotation and  $\mu_0$  is the magnetic permeability. The ratio  $Pm Pr^{-1}$  is also called the Roberts number,  $q$ . Among the parameters in (2),  $E$  gives the ratio of viscous to Coriolis forces,  $Ra$  gives the ratio of buoyancy to viscous forces and  $\Lambda$  gives the ratio of Lorentz to Coriolis forces.

Table I summarizes the range of parameters that our set-up can achieve and those relevant to the cores of Earth, Ganymede and Mercury. The non-dimensional numbers of the experiment are calculated using the inner

radius of the dome 0.138m as the characteristic length-scale  $d$  and angular velocity  $\Omega$  varying in the range  $[\pi/2 - 4\pi]$  rad s<sup>-1</sup>. The experimental Ekman number and both Prandtl numbers are out of geophysical range. This is a consequence of using a transparent liquid instead of liquid metal and having a small dome. The actual geophysical values of these parameters will remain out of the reach of numerical simulations or experiments for the foreseeable future. Concerning the Ekman number, our recent work shows that convection near the onset may reach an asymptotic regime for  $E \lesssim 10^{-5}$ , a value within reach of our apparatus [21].

In convection-driven planetary dynamos, the magnetic field generated by induction gives rise to a Lorentz force that in turn affects the structure of the flow at saturation. Magnetconvection focuses on the back reaction of the field on the flow rather than the generation of the mean field itself. Nevertheless, the convective flow observed in the experiment is likely to adopt a behaviour very similar to that expected in planetary cores. Finally, since our electrolyte-based system achieves a range of Elsasser numbers relevant to Earth and planetary cores, visual measurements of this rotating MHD regime are possible for the first time in a laboratory experiment.

### III. INSTRUMENTATION

We measure two quantities: the temperature and the velocity field. The temperature is measured with thermocouples and the velocity field is obtained by PIV.

#### A. Temperature measurement

To measure the temperature, we use four K-type thermocouples connected to a Pico TC-08 USB thermocouple data logger. The data resolution is 0.025 K. The thermocouples give the temperature near the surface of the heating element (1 mm below the interface of the ceramic plate and sulphuric acid), on the outside top of the dome, at the fluid inlet of the heating element, and at the outlet of the heating element. With these four measurements, we are able to monitor the imposed temperature difference  $\Delta T$  (see section II C) can be monitored. Since the flow rate of the heating fluid is precisely set by the peristaltic pump, the inlet and outlet temperatures give a precise measure of heat flux  $Q$  released by the heating element into the fluid. The temperature difference and heat flux respectively give the Rayleigh and Nusselt numbers. The Nusselt number is given by

$$Nu = \frac{QD}{k\Delta T} \quad (3)$$

where  $D$  is the fluid layer height above the heating element and  $k$  is the thermal conductivity of the working fluid.

#### B. PIV visualisation

To record the velocity field, a bespoke PIV system has been developed. This experimental technique has been commonly used with transparent fluids but the specific constraints of our apparatus (accessibility, rotation, influence of the magnetic field and risks associated to sulphuric acid) make its implementation particularly unusual. The principle of PIV is to seed the fluid with very small, neutrally buoyant non-inertial, highly reflective particles. These are then illuminated with a laser sheet. The resulting field of brightness is then recorded in a series of frames. The velocity field is obtained by calculating correlations between two successive frames [23]. Given our external constraints, we use a continuous, low-power (180mW) diode laser (532 nm) that is battery-operated. The tracer particles are silver coated glass spheres of size 13 $\mu$ m. Once the particles are well mixed in the fluid, we shine a laser sheet of thickness  $3.5 \pm 0.5$ mm into the measurement region. The laser is modified to separate the diode (positioned inside the magnet bore, outside the outer cylindrical shell, see figure 1) from its electronic controller (placed on the rotating acquisition platform, outside the region of intense magnetic field). The interaction between the laser plane and the particles produces localised areas of high light intensity. Images are captured at 20 frames per second by a charge coupled device (CCD) camera (Point Grey model FL3-FW-03S1C-C) with Sony ICX618 CCD, 1/4", 5.6  $\mu$ m sensor. The camera placed on the rotating acquisition table captures images from above the main cell, either directly or through a mirror fitted outside the cylindrical shell, at the desired height.

This set-up provides two types of measurements, in a vertical plane passing through the centre of the hemisphere and in horizontal planes parallel to the base. The vertical plane provides radial and axial velocity components,  $u_s(s, z)$  and  $u_z(s, z)$  at a prescribed azimuthal angle  $\phi$ , while the horizontal planes provide radial and azimuthal velocities  $u_s(s, \phi)$  and  $u_\phi(s, \phi)$  at a prescribed height  $z$  in a cylindrical polar coordinate system  $(s, \phi, z)$ . While varying  $z$  reveals different areas of the tangent cylinder, the flow inside the tangent cylinder is expected to be statistically axisymmetric under a uniform magnetic field. Hence the laser can be positioned at several heights  $z$  and one azimuthal angle.

Velocities in the vertical plane provide us with the size of the convective structure in the radial and axial directions above the heater. This is the preferred measurement to characterise the onset of convection and to observe upwelling motions. Azimuthal velocities measured in the horizontal planes give information on the structure of the azimuthal wind and polar vortices.



Control parameters	Water	$H_2SO_4$	Earth	Mercury	Ganymede
$E = \nu/\Omega d^2$	$[1.25 \times 10^{-5} - 1.25 \times 10^{-6}]$	$[4.51 \times 10^{-5} - 4.51 \times 10^{-6}]$	$10^{-15}$	$10^{-12}$	$10^{-13}$
$Ra = g\alpha\Delta T d^3/\kappa\nu$	$[2.09 \times 10^7 - 2.93 \times 10^9]$	$[1.4 \times 10^7 - 2.25 \times 10^9]$	$[10^{22} - 10^{30}]$	-	-
$\Lambda = B^2/\mu_0\rho\eta\Omega$	0	$[0 - 1]$	$[0.1 - 1]$	$10^{-5}$	$10^{-3}$
$Pr = \kappa/\nu$	7	12	$10^{-2}$	0.1	0.1
$Pm = \nu/\eta$	$\infty$	$10^{-10}$	$10^{-6}$	$10^{-6}$	$10^{-6}$

TABLE I: Range of achievable parameters in the experiment and comparison with planetary parameters. Note that the values of  $Ra$  are highly uncertain [22].

### C. Experimental procedure

Since the apparatus has a total height of 5m, alignment of rotating parts is critical, although the set-up is designed to operate under a small axial misalignment of 5 mm. To avoid air bubbles inside the glass dome, the outer cylinder is first filled with sulphuric acid up to a level higher than the dome diameter. The dome is then turned upside down, tilted and positioned on the turntable below the acid surface. The volume of acid remaining on the top of the dome is then pumped out and replaced with water. We then inject a mixture of  $H_2SO_4$  and silver-coated tracer particles inside the dome through pressure-release valves connected to the turntable. Operation starts by ramping up the magnetic field to a prescribed value. We then rotate the system until the fluid reaches solid body rotation, which takes approximately 30 minutes. The heating system is then activated, by first starting the pump to circulate the heating fluid, and then imposing a set voltage on the static heater to maintain the fluid temperature at a pre-determined value. Temperature and velocity measurements are then taken by remotely activating both the PIV system and the thermocouple data loggers via the mobile workstation mounted on the data acquisition platform.

## IV. EVIDENCE OF MAGNETICALLY CONTROLLED CONVECTION IN THE TANGENT CYLINDER

Figure 7 and 8 show contours of axial velocity in the vertical plane averaged in time at a fixed Ekman number of  $E = 1.3 \times 10^{-5}$  for  $\Lambda = 0$  and  $\Lambda = 0.1$ . Both cases exhibit clear upwelling and downwelling regions in well defined convective plumes. Their radial size is found by searching the radial distance corresponding to the first zero of the longitudinal correlation of radial velocity (see figure 9). Convection without magnetic field exhibits spiral structures akin to those first identified by [24] and theoretically predicted in [25], with a radial size  $l_r = 0.15$ , with  $l_r$  defined as the ratio of the structure size to the diameter of the heating element. By contrast, the magnetic case at  $\Lambda = 0.1$  features a much larger structure size  $l_r = 0.27$ . In the non-magnetic case, the radial size of the plumes is consistent with observations [24] and with prediction of the unstable mode responsible for the

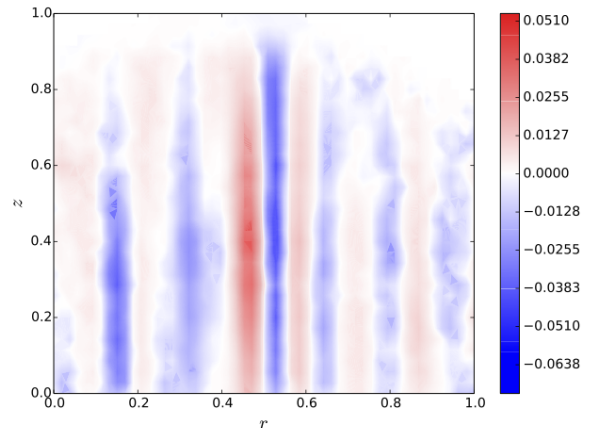


FIG. 7: Contours of the axial velocity  $u_z(r, z)$  for  $E = 1.15 \times 10^{-5}$ ,  $\Lambda = 0$  and  $Ra = 5.8 \times 10^{-5}$ .

onset of convection in a solid rotating cylinder heated from below [25] of the same aspect ratio as the tangent cylinder. Ours is the first study in this configuration under an imposed axial magnetic field. Hence no results exist for direct comparison. Nevertheless, the size of the thermal plumes in the magnetic case is consistent with that predicted for the onset of plane magnetoconvection. Indeed, the increase in lengthscale  $l_r$  with the magnetic field indicates an overall reduction in wavenumber of convection, in line with classical linear theory for onset in an infinite plane layer [6, 10, 21].

The thickening of convective plumes by an external magnetic field had been observed in a mercury experiment between two horizontal planes by Nakagawa [10], but our set-up provides the first full mapping of the convective structures. Additionally, it confirms that MHD effects can be reproduced in electrolytes and thus opens the way to a new range of experiments where visualisation can be achieved by means of transparent electrolytes in extremely high magnetic fields.

## V. CONCLUSION

The Little Earth Experiment introduces a new concept in the field of geophysical experiments relevant to liquid planetary cores. For the first time, the Magnetic-

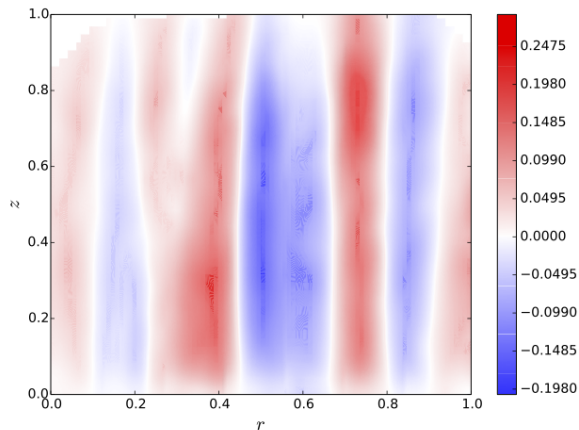


FIG. 8: Contour of the axial velocity  $u_z(r, z)$  for  $E = 1.15 \times 10^{-5}$ ,  $\Lambda = 0.33$  and  $Ra = 5.6 \times 10^{-5}$ .

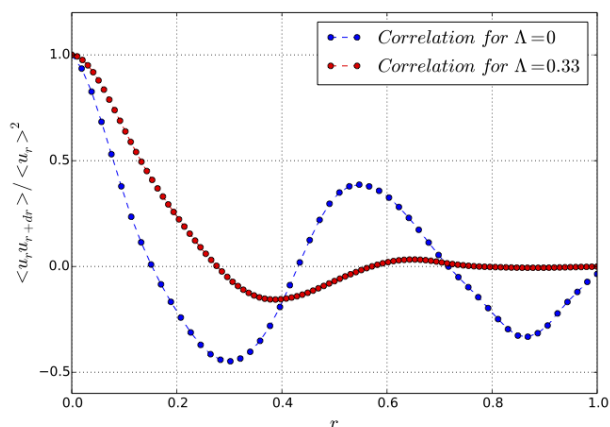


FIG. 9: Correlation function showing the thickening of the flow structure in the radial direction under an imposed axial magnetic field.

Archimedean-Coriolis (MAC) forces can be produced and precisely controlled in a flow that can also be fully mapped by means of optical visualisation techniques. This is achieved by replacing highly conductive but opaque liquid metals with transparent but weakly

conductive electrolytes (amongst which sulphuric acid achieves the best conductivity). The  $10^4$  factor lost in conductivity is compensated by magnets capable of delivering fields about 100 times higher than classical electromagnets, thus achieving a Lorentz force of the same order of magnitude as in liquid metals. This strategy is only made possible by the high field magnets available at the High Magnetic Field Laboratory, which are the only magnets with a bore large enough to accommodate fluid mechanics experiments.

The results presented here make two important points: First, this strategy is successful and coupled magnetohydrodynamic flows can indeed be reproduced in sulphuric acid and high magnetic fields. Second, the magnetic field has a spectacular effect on the structure of convective plumes, and both viscous and magnetic modes of convection observed in more ideal configurations [10] may take place in a range of Elsasser and Rayleigh numbers relevant to the Earth's core tangent cylinder.

Finally, the Little Earth Experiment is a very flexible set-up that can be easily adapted to a large variety of configurations: the core can be made smaller or larger, and the heater can impose a temperature or a heat flux at the solid-liquid boundary. Outer thermal boundary conditions could be varied with little modifications too. If the set-up is rotated faster than currently, convection would be driven in the radial direction outside the tangent cylinder. Finally, as the magnetic field in the Earth's tangent cylinder is not spatially uniform, experiments with inhomogeneous magnetic fields would reveal whether the convection pattern generated is consistent with that inferred from observation of the geomagnetic field and its secular variation [2, 26] and nonlinear dynamo simulations [5].

KA, AP, IB and BS acknowledge support from the Leverhulme Trust for this project (Research Grant RPG-2012-456), AP acknowledges support from the Royal Society under the Wolfson Research Merit Award scheme. The authors are indebted to the LNCMI and its technical and academic staff for the quality and effectiveness of their support. Access to the magnets was granted by the "Consortium de Recherche pour l'Emergence de Technologies Avancées" (CRETA) and the "Laboratoire National de Champs Magnetiques Intenses" (LNCMI), both part of the CNRS in Grenoble.

- 
- [1] Peter Olson and Jonathan Aurnou. A polar vortex in the earth's core. *Nature*, 402(6758):170–173, 1999.
  - [2] Gauthier Hulot, Céline Eymin, Benoît Langlais, Mioara Manda, and Nils Olsen. Small-scale structure of the geodynamo inferred from oersted and magsat satellite data. *Nature*, 416(6881):620–623, 2002.
  - [3] J. Aurnou, S. Andreadis, L. Zhu, and P. Olson. Experiments on convection in Earth's core tangent cylinder. *Earth Planet. Sci. Lett.*, 212(1):119–134, 2003.
  - [4] Binod Sreenivasan and Chris A Jones. Structure and dynamics of the polar vortex in the earth's core. *Geophysical research letters*, 32(20), 2005.
  - [5] B. Sreenivasan and C. A. Jones. Azimuthal winds, convection and dynamo action in the polar regions of planetary cores. *Geophys. Astrophys. Fluid Dyn.*, 100(4-5):319–339, 2006.
  - [6] S. Chandrasekhar. *Hydrodynamic and hydromagnetic stability*. Clarendon Press, Oxford, 1961.



- [7] J Pedlosky. Geophysical fluid mechanics, 1987.
- [8] B. Sreenivasan and C. A. Jones. Structure and dynamics of the polar vortex in the earth’s core. *Geophys. Res. Lett.*, 32:L20301, 2005.
- [9] K Jirlow. Experimental investigation of the inhibition of convection by a magnetic field. *Tellus*, 8(2):252–253, 1956.
- [10] Y. Nakagawa. Experiments on the instability of a layer of mercury heated from below and subject to the simultaneous action of a magnetic field and rotation. *Proc. R. Soc. A*, 242(1228):81–88, 1957.
- [11] O Andreev, A Thess, and Ch Haberstroh. Visualization of magnetoconvection. *Physics of Fluids (1994-present)*, 15(12):3886–3889, 2003.
- [12] J. M. Aurnou and P. L. Olson. Experiments on Rayleigh–Bénard convection, magnetoconvection and rotating magnetoconvection in liquid gallium. *J. Fluid Mech.*, 430:283–307, 2001.
- [13] CA Jones. Convection–driven geodynamo models. *Philosophical Transactions of the Royal Society of London A: Mathematical, Physical and Engineering Sciences*, 358(1768):873–897, 2000.
- [14] Ulrich R Christensen and Johannes Wicht. Numerical dynamo simulations. In *Core Dynamics*, pages 245–282. Elsevier, 2007.
- [15] Binod Sreenivasan, Swarandeeep Sahoo, and Gaurav Dhama. The role of buoyancy in polarity reversals of the geodynamo. *Geophysical Journal International*, 199(3):1698–1708, 2014.
- [16] JB Taylor. The magneto-hydrodynamics of a rotating fluid and the earth’s dynamo problem. In *Proceedings of the Royal Society of London A: Mathematical, Physical and Engineering Sciences*, volume 274, pages 274–283. The Royal Society, 1963.
- [17] SI Braginsky. On the nearly axially-symmetrical model of the hydromagnetic dynamo of the earth. *Physics of the Earth and Planetary Interiors*, 11(3):191–199, 1976.
- [18] M NECATI Ozisik. Heat conductionwiley. *New York*, page 63, 1980.
- [19] Oleg Andreev, Yurii Kolesnikov, and André Thess. Visualization of the ludford column. *Journal of Fluid Mechanics*, 721:438–453, 2013.
- [20] Horace E Darling. Conductivity of sulfuric acid solutions. *Journal of Chemical & Engineering Data*, 9(3):421–426, 1964.
- [21] Kélig Aujogue, Alban Pothérat, and Binod Sreenivasan. Onset of plane layer magnetoconvection at low ekman number. *Physics of Fluids (1994-present)*, 27(10):106602, 2015.
- [22] G Schubert and KM Soderlund. Planetary magnetic fields: Observations and models. *Physics of the Earth and Planetary Interiors*, 187(3):92–108, 2011.
- [23] Markus Raffel, Christian E Willert, Jürgen Kompenhans, et al. *Particle image velocimetry: a practical guide*. Springer, 2013.
- [24] Fang Zhong, Robert Ecke, and Victor Steinberg. Asymmetric modes and the transition to vortex structures in rotating rayleigh–bénard convection. *Physical review letters*, 67(18):2473, 1991.
- [25] HF Goldstein, E Knobloch, I Mercader, and M Net. Convection in a rotating cylinder. part 1 linear theory for moderate prandtl numbers. *Journal of Fluid Mechanics*, 248:583–604, 1993.
- [26] Andrew Jackson, Art RT Jonkers, and Matthew R Walker. Four centuries of geomagnetic secular variation from historical records. *Philosophical Transactions of the Royal Society of London A: Mathematical, Physical and Engineering Sciences*, 358(1768):957–990, 2000.